CrossMark

ORIGINAL PAPER

Rock burst assessment in multi-seam mining: a case study

Wei Shen[1,2] · Lin-ming Dou[1,2] · Hu He[3] · Guang-an Zhu[1,2]

Abstract To assess rock burst prone zones in the lower seam during multi-seam mining, a rock burst hazard assessment method for use in multi-seam mining was established. According to the observed geological evolution, the feasibility of using upper layer coal mining data to determine the rock burst risk zone of the lower coal seam is explained. Then, we established the energy density risk index (EDRI) and proved that the EDRI more accurately reflected the potential rock burst region than the multi-factor coupling analysis method. Finally, we established the rock burst hazard assessment method for use in multi-seam mining by using the EDRI of the upper coal to divide the rock burst risk zone in the lower coal. From the accuracy and validity analysis of this assessment method, we find that the critical energy induced rock burst, and the damage area of a rock burst in the lower coal seam were all located in the high-risk zone derived from this assessment method. To quantify the effectiveness and practicability of this assessment method, the structural similarity (SSIM) index, from image quality assessment research, was introduced. The SSIM index between predicted-high-risk map and actual high-risk map index was 0.8581, which shows that the established rock burst hazard assessment method in multi-seam mining can be used to predict rock burst risk zones in the lower seam.

Keywords Energy density risk index (EDRI) · Structural similarity (SSIM), multi-coal seam · Rock burst risk zone assessment

Introduction

With the increase of depth and intensity, the rock burst damage range and intensity have been increasing significantly (Braeuner 1994; Dou et al. 2012; Jiang et al. 2014). Each year, rock bursts cause considerable economic loss and enormous casualties. For instance, on February 14, 2005, as the rock burst caused a serious gas explosion, 214 people were killed in Sunjiawan Coal Mine in Fuxin, Liaoning Province, China (Li et al. 2015).

Forecasting rock burst hazard regions is a prerequisite for rock burst control. Many traditional methods of evaluating rock burst hazard have been proposed, such as seismic energy and event correlations, velocity tomography, the aggregate index, and multifactor coupling (Dou et al. 2006; Dou et al. 2014; Eneva et al. 1998; Chen et al. 2012; Peng et al. 2002; Zhao et al. 2000). As micro seismic systems can accurately, and constantly, reflect the cracking, stresses in the coal and surrounding rock and geologic structures, they are widely used to assess rock burst hazard. Many scholars have verified the correlation between seismic events and stress. (Kracke and Heinrich 2004; Abdul-Wahed et al. 2006; Srinivasan et al. 1997; Driad-Lebeau et al. 2005). Since a power-law relationship is found between the P-wave velocity and stress, seismic velocity tomography based on a micro-seismic system has been used in various fields. It is confirmed that seismic hazard

✉ Lin-ming Dou
lmdou@cumt.edu.cn

Wei Shen
826618111@qq.com

1 Key Laboratory of Deep Coal Resource Mining, Ministry of Education of China, School of Mines, China University of Mining & Technology, Xuzhou, Jiangsu 221116, China

2 School of Mines, China University of Mining and Technology, Xuzhou, Jiangsu 221116, China

3 School of Resources and Earth Science, China University of Mining and Technology, Xuzhou, Jiangsu 221116, China

zones and high abutment stresses are combined not only with zones of high velocity values, but also with zones of high velocity gradient values. (Lurka 2005; Gong et al. 2012a, b).

Although micro-seismic methods have been proposed to assess rock burst hazard, there are no seismic data records where a coal seam has not been mined, and in that situation, we can only use the aggregate index and multi-factor coupling instead of micro-seismic methods. The aggregate index and multi-factor coupling methods are empirical; they consider many extrinsic factors related to rock bursts. For example, mining depth, the mechanical properties of both coal and rock masses, the structural features of both floor and roof, variations in coal seam thickness, faulting, geological structure, and overall disposition of the working faces (Bukowska 2006). Under the influence of the same extrinsic factors, such as faulting, the stress concentration coefficient of two faults may differ significantly. The concentration coefficient of one may be 2, however, that of the other may be 1, or even less. The rock burst hazard zones obtained by these empirical methods do not always match the cases seen in actual mines (Zhang et al. 2013). The aggregate index and multi-factor coupling based on the empirical analogy method suffer from this limitation and is subject to even bigger errors when it is used to rock burst hazard evaluation.

Aiming at multi seam mining, we used micro-seismic data to establish the energy density risk index (EDRI), and proved that the EDRI was more able to reflect the potential rock burst region more accurately than the multi-factor coupling analysis method. Then a rock burst hazard assessment method for use in multi-seam mining was established according to the experience analogy method. Eventually, we introduced the SSIM to quantify the effectiveness and practicability of this assessment method.

Evaluation method

The feasibility of evaluation

In the generation of rock structure, and mineral composition, rocks are changed under the actions of alteration and weathering, which lead to inhomogeneity in geologic media. Various structural planes, such as faults, are formed under the action of tectonic movement, which results in discontinuities in the rock. Some rock stress boundaries are relieved, and the other rock stresses are locked-in during geological evolution, which leads to differences in the stress distributions therein.

With the increase of rock mass size, the physical properties and mechanical properties of rock will become more complicated. The theoretical results usually show significant deviation from actual data and the empirical analogy method is more practical than theoretical calculation in geotechnical engineering practice.

The strata in this coal mine are almost all sedimentary rocks. The area of the coal seam covers several square kilometres or even several hundreds of square kilometres. Differences in the physical properties of the rocks and their surrounding environment are readily seen at such a large scale, and the accuracy of any empirical analogy is greatly reduced. Conversely, compared with the horizontal direction, the distance between the strata is small, and differences in the vertical direction are small. Therefore, it is reasonable to determine the rock burst hazard zone in the lower coal seam by using monitored data from the upper coal seam.

Establishment of evaluation method

(1) The energy density risk index

According to rock mechanics theory, a shock event is defined as a sudden inelastic deformation within a certain volume which causes detectable vibration waves (Cai et al. 2014). The energy released by each tremor is proportional to the square of the strain in the rock before the tremor, and the strain is directly proportional to the stress in the elastic stage. Therefore, strain energy could reflect the stress state before a tremor (Benioff 1951; Kracke and Heinrich 2004). Friedel et al. (1995, 1997) and Bańka and Jaworski (2010) proved that the energy released by tremors is positively correlated with stress, and the tremors are closely related to rock burst occurrence.

Seismic events were considered as point sources when calculating earthquake, tremor, or source locations (Frankel 1995; Frankel et al. 2000), which could not be directly reflected by the magnitude of the energy in a certain region. Here, the EDRI method was proposed to assess the tremor characteristics of a region.

The tremor energy E, which was obtained from the micro-seismic monitoring system, was used in (1) to obtain the energy per unit area. As the energy in a large tremor was thousands, or even millions, of times than that of a small tremor, differences among low-energy tremors were hard to resolve. By drawing lessons from the method of using the earthquake magnitude ($M \propto \log_{10}E$) to express to earthquake intensity in seismology, the energy index was used to represent the magnitude of the energy, which could be obtained by using (2). According to the theoretical analysis, laboratory experiments and a large number of field tests (Dou and He 2007), the risk level associated with a tremor was quantified into four grades (Table 1). Therefore, the EDRI, which was obtained by normalising formula (3), was divided into four grades. The EDRI varies from zero to one and was sub-divided into four categories: $0 \leq EDRI < 0.25$, $0.25 \leq EDRI < 0.5$, $0.5 \leq EDRI < 0.75$, and $0.75 \leq EDRI \leq 1$, respectively, indicating no risk, weak risk, moderate risk, and high risk.

Consequently, the risk evaluation criterion for a rock burst is established (Table 1).

$$E_i = \frac{\sum E_j}{A} \quad (1)$$

$$e_i = \log_{10}(E_i) \quad (2)$$

$$EDRI_i = \frac{e_i - e_{min}}{e_{max} - e_{min}} \quad (3)$$

Where E_i is the energy value per unit area of the ith statistical region, $\sum E_j$ represents the total energy of the jth seismic event in the ith statistical region, and A is the area of the ith statistical region, m^2; e_i is the energy index of the ith statistical region, $\log 10(J)$, e_{max} is the maximum value of all e_i, e_{min} is the minimum value of all e_i, and $EDRI_i$ denotes the energy density risk index of the ith statistical region.

To reduce the range between the maximum and minimum values of the energy index, the average of the five biggest values was set to e_{max}, and the average of the five minimum values was set to e_{min}.

(2) Generation of the EDRI

To map the EDRI, the sketch map of the spatial, statistically smoothed model was established, as shown in Fig. 1. Seismic events belonging to each statistical region are selected to calculate the EDRI using Eqs. (1), (2), and (3), which are then considered as the value at its corresponding grid node. Finally, the EDRI map can be generated by interpolation. To avoid a lack of fidelity in the results induced by omitting individual seismic events, the relationship between the grid spacing S and the statistically smoothed radius R should satisfy: $S \le \sqrt{2} R$ (Cai et al. 2015). The statistically smoothed radius R was determined by the hypocentre location error calculated by the numerical emulation method in the process of the statistical calculation (Gong et al. 2010). The map of hypocentre location errors is shown in Fig. 2: the hypocentre location error of the working face under investigation was less than 20 m. So, the statistically smoothed radius R of 20 m could be obtained, and grid spacing S was set to 28 m accordingly.

Table 1 Relationship between the energy density risk index and rock burst risk

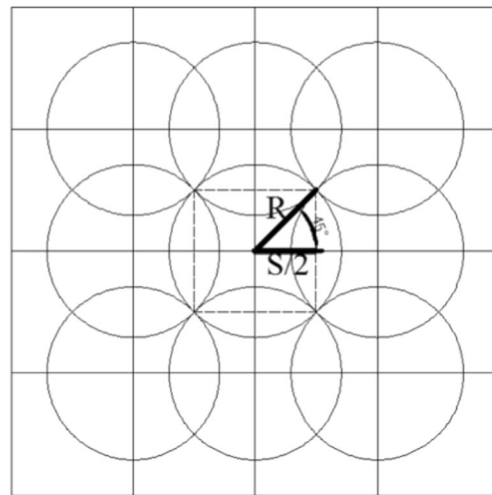| Risk rate	Rock burst risk	Abnormal value	EDRI
A	None	<0.25	$0 \le EDRI < 0.25$
B	Weak	0.25~0.5	$0.25 \le EDRI < 0.5$
C	Moderate	0.5~0.75	$0.5 \le EDRI < 0.75$
D	Strong	>0.75	$0.75 \le EDRI \le 1$

Fig. 1 Sketch map of the spatial, statistically smoothed model: S is the grid spacing and R is the statistically smoothed radius such that $S \le \sqrt{2} R$

The validity of the evaluation method

To quantify the effectiveness of the prediction method, we introduced structural similarity theory to calculate the similarity ratio between the predicted rock burst risk map and the actual rock burst risk map.

Under the assumption that human visual perception is highly adapted for extracting structural information from a scene, an alternative complementary framework is used for quality assessment based on the degradation of structural information. Structural similarity indexing is a specific example of this concept (Wang et al. 2004). Structural similarity index, which is a particular implementation of the philosophy of structural similarity, reflects the properties of object brightness, contrast, and structure. The index of structural similarity is defined (in (4)) as

$$SSIM(X, Y) = \frac{\left(2\mu_x\mu_y + C_1\right)\left(2\sigma_{xy} + C_2\right)}{\left(\mu_x^2 + \mu_y^2 + C_1\right)\left(\sigma_x^2 + \sigma_x^2 + C_2\right)} \quad (4)$$

where μ_x and μ_y are the mean values of image signals X and Y, respectively, estimated as the signal luminance; σ_x and σ_y are the standard deviations, estimated as the signal contrast; σ_{xy} is the covariance, estimated as the signal structure; $C_1 = (K_1 L)^2$ and $C_2 = (K_2 L)^2$, L is the dynamic range of the pixel values, $K_1 = 0.01$ and $K_2 = 0.03$ by default (Wang et al. 2004).

When the two images are the same, the value of the SSIM index is one (its maximum value): the larger the value of the SSIM index, the greater the consistency of the two images.

Fig. 2 The map of hypocentre location error
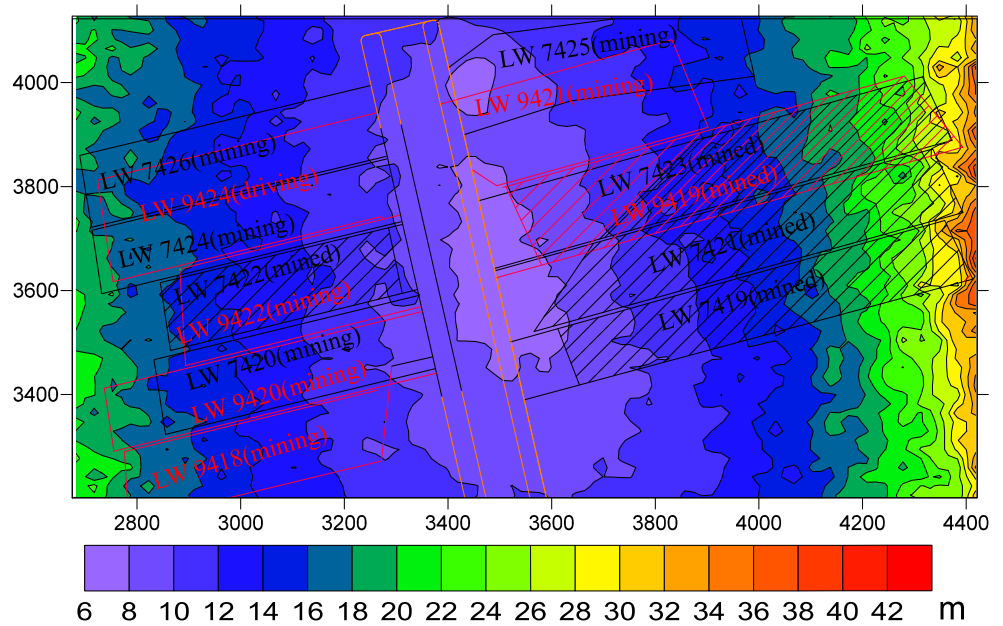
Case study

Site description

The Zhangshuanglou coal mine is located in the northwest of Jiangsu Province, China. The study area was chosen as the west district of the coal mine. Seams 7 and 9, whose seam dips are 25°, formed the main mineable coalbed. The strata between two seams comprise 3 m of mudstone and 20 m of sandstone. The working faces in this district are at depths ranging from 970 to 1100 m. Caving mining was adopted throughout this district, and the No. 7 seam mining is a priority for excavation compared to the No. 9 seam. The KJ20 microseismic system, which includes three groups of 3-component (Nos. 1, 2, and 3) probes and one group of 1-component probes (Nos. 4, 5, and 6), was installed by Xilin Ltd. on 6 April 2011. Before installation, LW7419, 421, 422, 423, and LW9419 had been mined. Fig. 3 shows the panel geometry and relative receiver locations.

The critical energy of a rock burst

(1) The discriminating method of critical value

When analysing the Gurtenberg-Richter power-law for earthquake, rock burst, and acoustic emissions, Amitrano et al. (2012) reports are deviating from the power-law at high energies. The inflexion point of the power-law relationship is regarded as the dividing line denoting high-energy shock, which can be treated as a critical value for a rock burst. The Gurtenberg-Richter power-law equation is as follows:

$$\lg N(\geq \lg E) = a - b\lg E \tag{5}$$

Where E is the energy of the shock; $N(\geq \lg E)$ is the number of shocks which are greater than, or equal to, E; and a and b are constant.

To identify the inflexion point of Gurtenberg-Richter power-er rate curve, the correlation coefficient is introduced here. According to the Gurtenberg-Richter power distribution equation, $\lg N$ and $\lg E$ are completely linearly correlated with a correlation coefficient R of 1 in theory. However, there is a certain deviation between $\lg N$ and $\lg E$, which are not a complete linearly correlation in reality (see Fig.4).

As the discreteness of tremors is large in the high-energy region, the correlation coefficient R decreases gradually with the increasing number of events for which the correlation coefficient R between $\lg N$ and $\lg E$ is calculated. After the energy fell below the inflexion point demarcating high- and low-energy tremors, the drift rate between $\lg N$ and $\lg E$ gradually decreased, which meant that the correlation coefficient R increased.

Therefore, the energy value corresponding to the minimum R can be used as the inflexion point demarcating high- and low-energy tremors. A tremor with an energy greater than the inflexion point are called The characteristic mining tremor. The characteristic mining tremor is statistically an abnormal shock, which is the critical energy required to induce a rock burst (Cai et al. 2014). The correlation coefficient is given by the following equation:

$$R_i = \frac{\sum_{j=i-1}^{n}\left(x_j-\overline{x}\right)\left(y_j-\overline{y}\right)}{\sqrt{\sum_{j=i-1}^{n}\left(x_j-\overline{x}\right)^2 \sum_{j=i-1}^{n}\left(y_j-\overline{y}\right)^2}} \tag{6}$$

Fig. 3 Layout of the micro-seismic monitoring system in the western district. **a** Plane graph. **b** Profile 1–1′. **c** Profile 2–2′
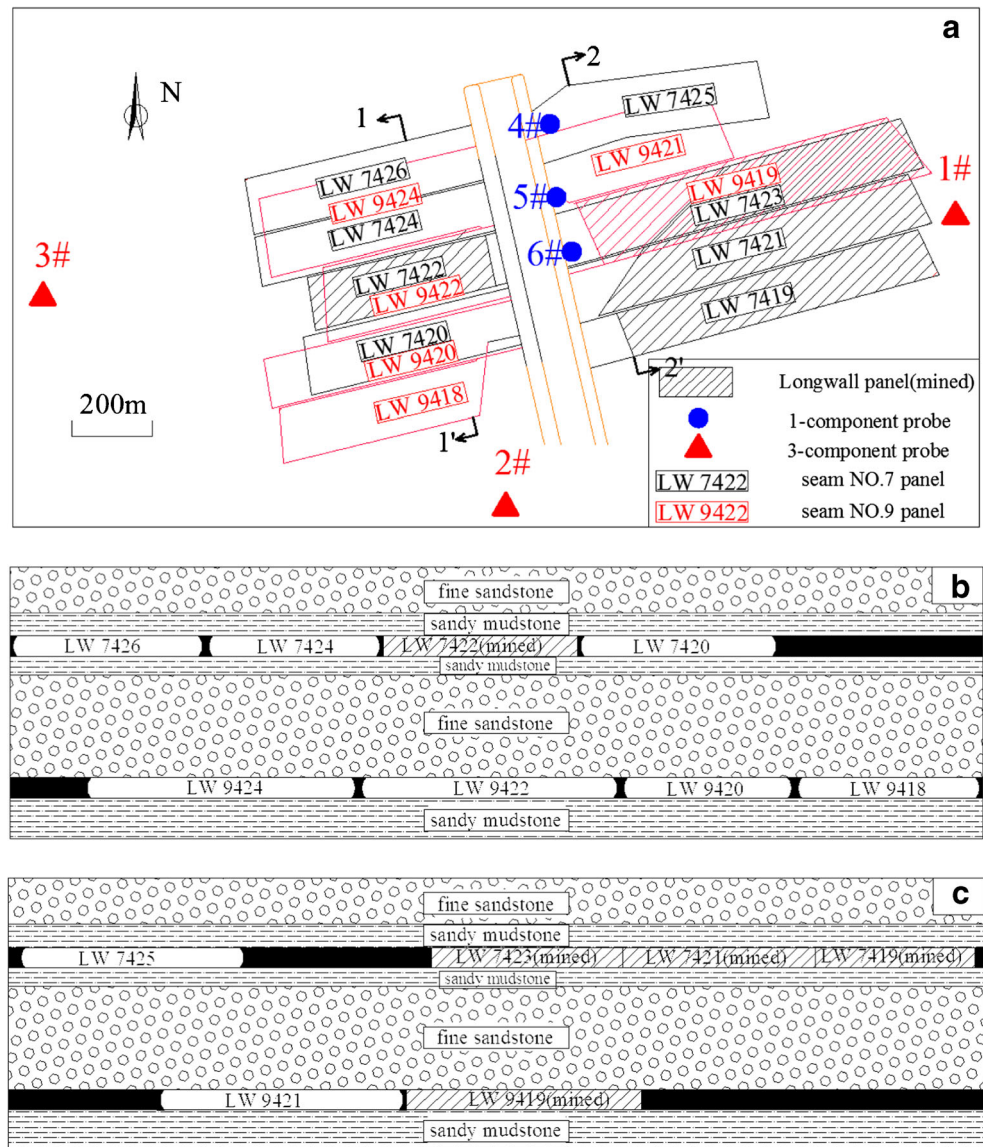
Where $i = 2, 3, \cdots, n$; R_i is the correlation coefficient for $\lg E_i$ in the Gurtenberg-Richter power-law curve; x is $\lg E_{i-1}$, $\lg$

E_i, $\lg E_{i+1}$, $\cdots$, $\lg E_n$; y was $\lg N_{i-1}$, $\lg N_i$, $\lg N_{i+1}$, $\cdots$, $\lg N_n$; $\overline{x}$ is the mean average of all x, and $\overline{y}$ is the average value of all y.
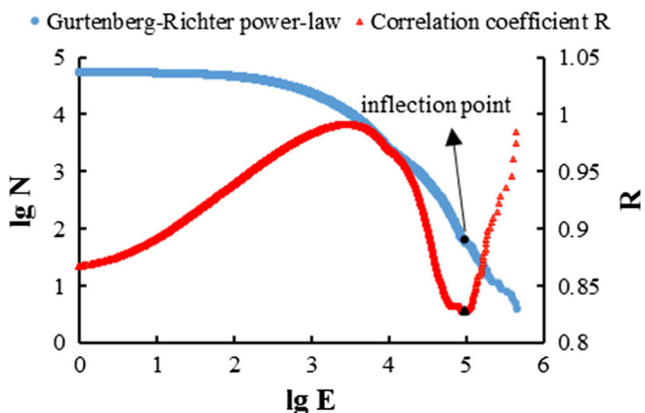
When $R_k = \min\left\{R_{\frac{n-1}{2}}, R_{\frac{n+1}{2}}, R_{\frac{n+3}{2}}, R_k, \cdots, R_n\right\}$, the corresponding point $(R_k, \lg E_k)$ is the inflexion point of the Gurtenberg-Richter power-law, and E_k is the critical energy required to induce a rock burst.

According to micro-seismic data from Zhangshuanglou coal mine, we can plot $\lg E - R$ and $\lg E - \lg N$ curves (Fig. 4). The shock energy corresponding to inflexion point of the Gurtenberg-Richter power-law was 10^5 J, therefore this was also the critical energy required to induce a rock burst.

(2) The energy of a rock burst

A rock burst is induced by the interaction of static and dynamic load regimes, and a large energy shock is needed

Fig. 4 $\lg E - R$ and $\lg E - \lg N$ curves

Table 2   The energy released by rock bursts in Zhangshuanglou coal mine

Rock burst	Date	Energy/J
1	30 July 2010	Unknown
2	27 Oct. 2012	4.46×10^5
3	10 Dec. 2012	4.34×10^5
4	30 Jan. 2014	1.24×10^5
5	23 Mar. 2014	1.21×10^5
6	7 Nov. 2014	1.68×10^5

to cause a rock burst (Dou et al. 2006). We could effectively forecast the potential risk zone associated with a rock burst by predicting the zone with high-energy shock risk. The micro-seismic monitoring system can record the waveform generated by rock mass fracture and record the energy and position of each high-energy shock. By using the seismic monitoring system, the data relating to rock bursts (since the coal mine was established) and the corresponding source energies of Zhang Shuanglou mine are listed in Table 2. The recorded energies inducing rock bursts all exceeded 1.0×10^5 J. The rock burst energy released on 30 July 2010 is unknown because the micro seismic monitoring system was not installed at that time. According to descriptions from site workers, the intensity and damage area exceeded any one rock burst occurring in Zhangshuanglou coal mine, so it was believed that the rock burst energy released on 30 July 2010 exceeded 1.0×10^5 J.

According to the field observation results, it was concluded that only energies exceeding 1.0×10^5 J could induce a rock burst, which confirmed the conclusion obtained in the last section.

The EDRI method and the multi-factor coupling method

Correlation between the EDRI and rock burst hazard

Figure 5 was obtained by the monitoring of seismic events in the mining process of coal seams Nos. 7 and 9 (except for panels LW7419, 421, 423, 422, and LW9419). Symbols show positions of tremors with an intensity exceeding 10^5 J, and Ellipses delineate the damage area induced by each rock burst.

According to the monitoring results, there were 20 tremors with an intensity above 10^5 J in this district during the mining process, and 19 of them were located in the high-risk zone. Moreover, all the damage regions of the four rock bursts were located in the high-risk zone. From the statistical results, it was concluded that the high-risk zone of EDRI map could reasonably and effectively forecast the critical shock and the damage zone of each rock burst. This matched previous results, in which microseismic activity recorded during mining, could pinpoint zones of a risk of rock bursting (Senfaute et al. 2014).

Comparison with the multi-factor coupling method

The multi-factor coupling analysis method is based on the effect of those rock burst influencing factors in a coal mine, such as faulting, folding, coal pillars, coal seam roadway intersections, mergers, and roof lithologies. Firstly, different influencing factors are used to determine the rock burst hazard zones. Then, the final rock burst hazard map is obtained by the superposition of each rock burst hazard zone. Multi-factor coupling analysis has been widely used in coal mine burst risk assessment (Dou et al.

Fig. 5 EDRI map. Four different colours were used to represent four risk grades of EDRI: the *light blue* zone (0 to 0.25), the *blue* zone (0.25 to 0.5), the *green* zone (0.5 to 0.75), and the *red* zone (0.75 to 1), respectively, representing no risk, weak risk, moderate risk, and high risk
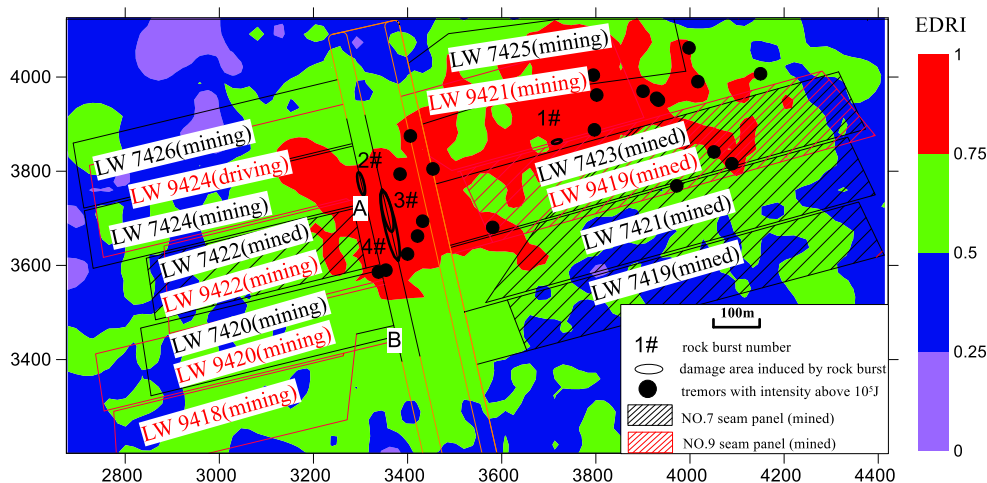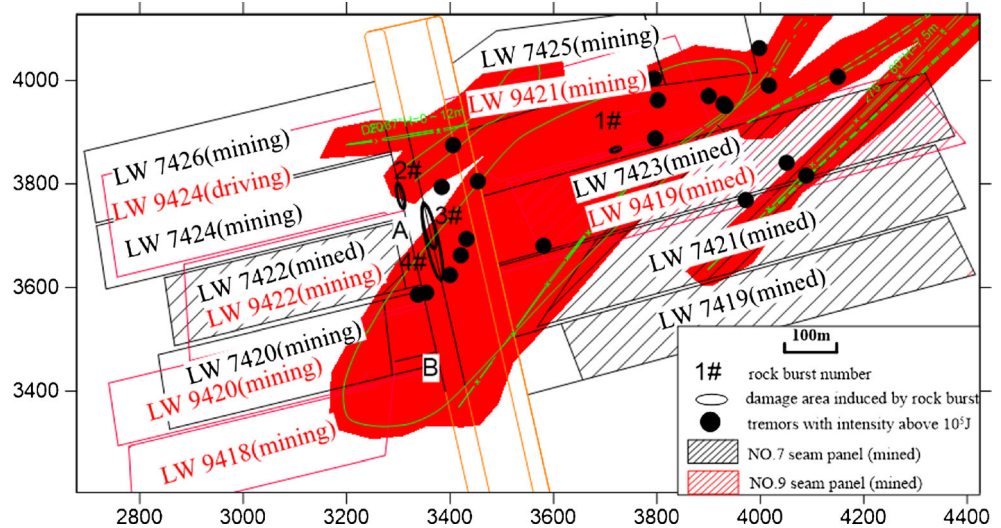
Fig. 6 The rock burst hazard zone found using the multi-factor coupling analysis method

2006, PATYNSKA 2013). According to the mining conditions prevailing in the research area, we can obtain the overall rock burst hazard map (Fig. 6) by using the multi-factor coupling analysis method.

As seen from Fig. 6, the critical shock and damage zone, of the rock burst, are located near the rock burst hazard zone, which suggested that the multi-factor coupling analysis method can be used to predict the hazard risk zone; however, compared to the EDRI, this method suffers from a large relative error. For example, there are damage areas induced by rock bursts occurring in region A, but that region was not a rock burst hazard zone according to the multi-factor coupling analysis method. There is no critical shock or damage in region A; however, region B was a rock burst hazard zone according to the multi-factor coupling analysis method.

Compared with the multi-factor coupling analysis method, the EDRI can more accurately reflect the rock burst risk.

Discussion of the validity of the evaluation method

Consistency between the evaluation data and critical tremors in the lower seam

As seen from Fig. 7, the map of EDRI, which was obtained by the monitoring of seismic events in the mining process of coal seam No. 7 (except for panel LW 7419, 421, 423, and 422), was used to predict the risk zone during the mining process of coal seam No. 9. Symbols

Fig. 7 Comparison of prejudged danger areas and critical tremors inducing rock bursts in the No. 9 seam
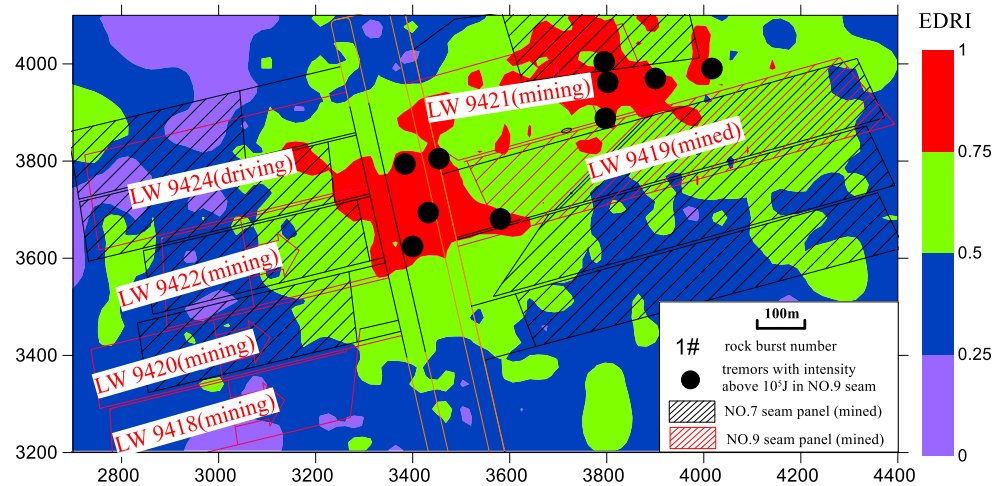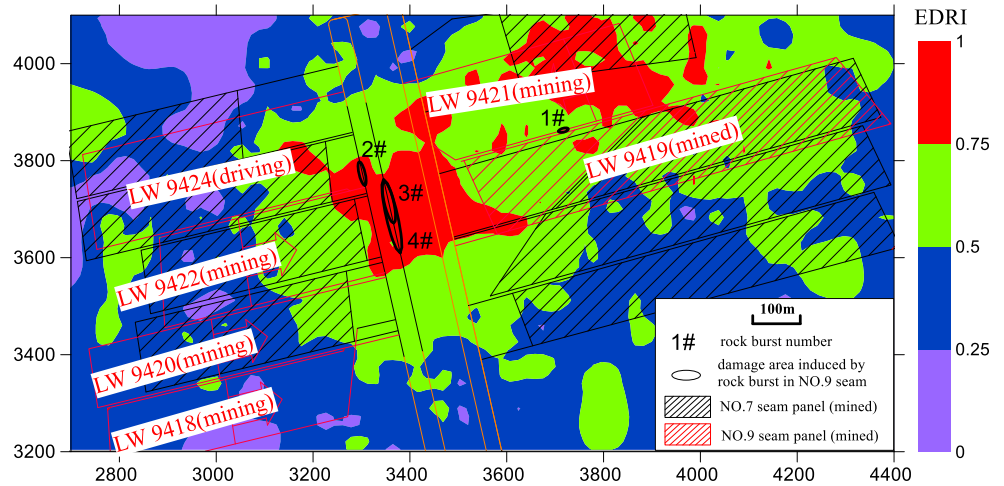
Fig. 8 Comparison of prejudged danger areas and the area damaged by rock bursts in seam No. 9

show positions of critical tremors in the mining process of the No. 9 seam.

There were a total of 10 critical tremors inducing rock bursts seen in this district during the mining of the No. 9 seam, and all of them were located in the high-risk zone. We can conclude that the established EDRI map of the upper seam could effectively predict the position, and extent, of critical tremors inducing rock bursts in the lower coal seam.
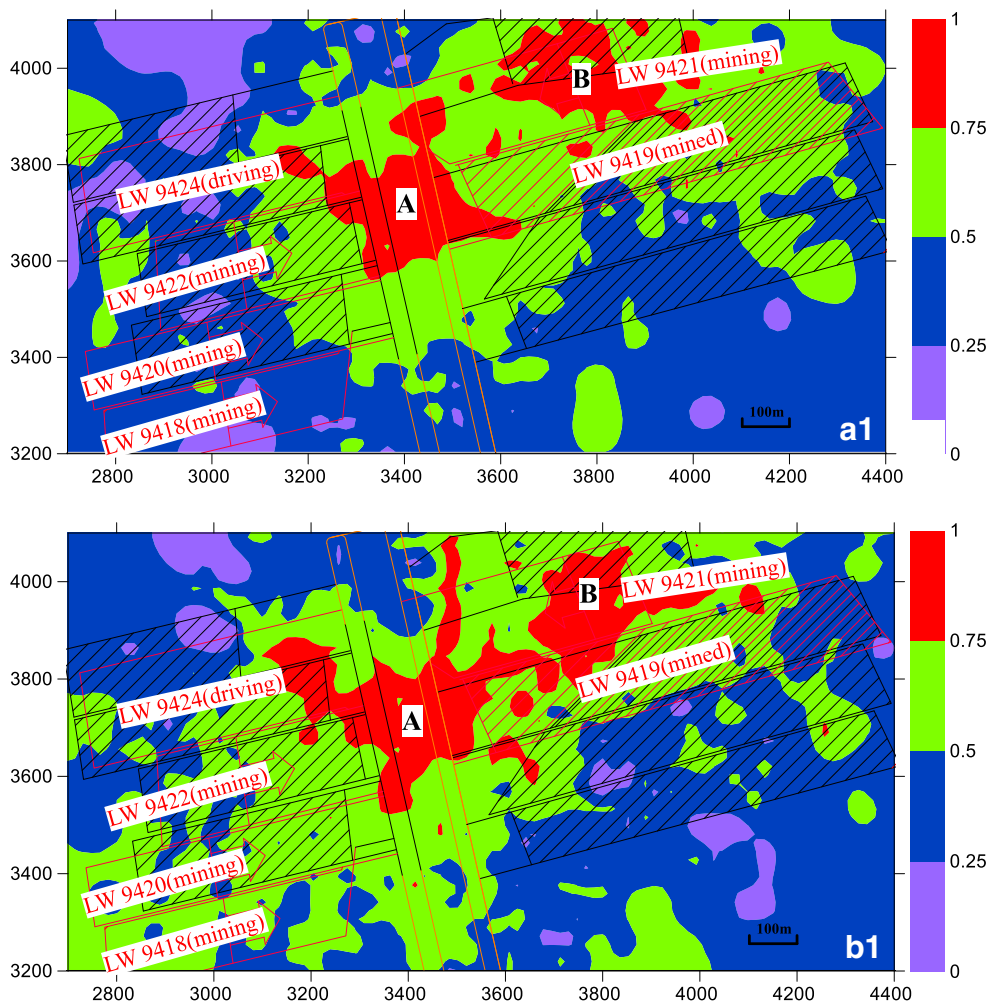

Fig. 9 Rock burst risk maps. (a1) Plan view of the predicted rock burst hazard zone. (a2) Plan view of the predicted high-risk zone. (b1) Plan view of the actual rock burst hazard zone. (b2) Plan view of the actual high-risk zone
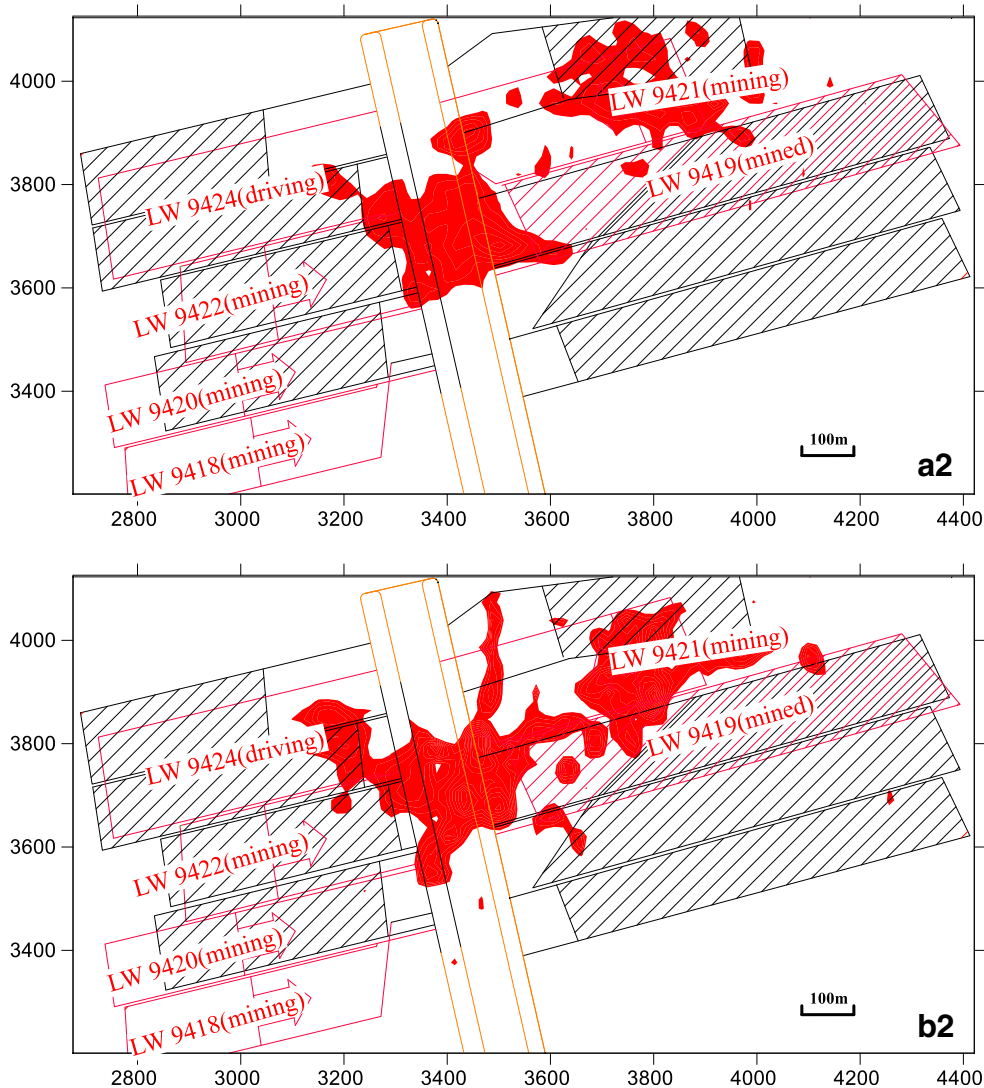
Fig. 9 (continued)

Consistency between the evaluation data and the rock burst-damaged area in the lower seam

As seen from Fig. 8, the map of EDRI, which was obtained by the monitoring of seismic events in the mining process of coal seam No. 7 (except for panels LW7419, 421, 423, and 422), was used to predict the risk zone during the mining process of coal seam No. 9. Ellipses delineate the damage area induced by each rock burst in the mining process of the No. 9 seam.

There were four rock bursts during mining of seam No. 9, with three rock bursts (Nos. 2, 3, and 4) located in high-risk zones on the EDRI map, as seen in Fig. 8. Coal in the vicinity of the first damaged area was not extracted during mining of the No. 7 seam. In contrast, the area was extracted during mining of the No. 9 seam, which increased the abutment stresses therein and induced the first rock burst.

From the above analysis, the rock burst damaged area of the lower coal seam can be predicted through the proposed assessment method. However, consideration should be given to the different mining disturbances between the two coal seams—increased mining disturbance will increase the rock burst hazard.

Quantitative evaluation

As seen from Fig. 9 *a1* and *a2*, the map of EDRI and high-risk zone of EDRI, which were obtained by the monitoring of

Table 3   SSIM data

Panel comparison	SSIM (all zones)	SSIM (high-risk zone)
Panel of predicted and actual zones	0.4726	0.8581

seismic events in the mining process of coal seam No. 7 (except for panels LW7419, 421, 423, and 422), were called the predicted risk map; in Fig. 9 *b1* and *b2*, the map of EDRI and high-risk zone of EDRI, which were obtained by the monitoring of seismic events in the mining process of coal seam No. 9 (except for panel LW9419), was called the actual risk map.

From Fig. 9, the predicted high-risk zones are located in regions A and B, and the actual high-risk zones are also located therein. Almost all of the zones in LW9418, 420, 422, and 424 were non-high-risk according to predicted risk results—the actual risk results showed a similar trend.

To quantify the similarity, SSIM is introduced. To ensure the assessment accuracy of the SSIM index between the predicted rock burst risk map and actual rock burst risk map in the No. 9 seam, images were cropped to the same size, and the same colour should be selected in the same risk section, as shown in Fig. 9. Table 3 lists the values of SSIM between the predicted and actual risk maps.

The value of SSIM between the predicted, and actual, rock burst risk maps is 0.4726 (see Fig. 9 *a1* and *a2*). However, the value of SSIM between the predicted high-risk zone and actual high-risk zone is 0.8581 (see Fig. 9 *b1* and *b2*).

It was concluded that the established rock burst hazard assessment method can accurately forecast the extent and position of the high-risk zone.

Conclusion

(1) According to the discriminating method of critical value and the field observation results, the critical energy required to induce a rock burst exceeded 1.0×10^5 J in each case, which confirmed the feasibility of the discriminating method of critical energy-induced rock burst prediction.

(2) Through practical application, the EDRI can accurately reflect rock burst risk to a better extent than the multi-factor coupling analysis method.

(3) All critical tremors induced rock bursts, and the damage zones induced by rock bursts in the lower coal seam were located in high-risk hazard zones, which were predicted by this rock burst hazard assessment method for use in multi-seam mining. The value of SSIM between the predicted high-risk zone and the actual high-risk zone is 0.8581, which indicates that the established rock burst hazard assessment method used in multi-seam mining can accurately forecast the extent and position of the high-risk zone.

References

Abdul-Wahed MK, Heib MA, Senfaute G (2006) Mining-induced seismicity: seismic measurement using multiplet approach and numerical modeling. Int J Coal Geol 66:137–147

Amitrano D, Gruber S, Girard L (2012) Evidence of frost-cracking inferred from acoustic emissions in a high-alpine rock-wall. Earth planet sci let 341–344(2):86–93

Bańka P, Jaworski A (2010) Possibility of more precise analytical prediction of rock mass energy changes with the use of passive seismic tomography readings. Arch Min Sci 55:723–731

Benioff H (1951) Crustal strain characteristics derived from earthquake sequences. Trans Am Geophys Union 32:508–514

Braeuner G (1994) Rockbursts in coal mines and their prevention. Crc Press, Boca Raton

Bukowska M (2006) The probability of rockburst occurrence in the upper Silesian Coal Basin area dependent on natural mining conditions. J Min Sci 42(6):570–577

Cai W, Dou LM, Li ZL, Liu J, Gong SY, He J (2014) Microseismic multidimensional information identification and spatio-temporal forecasting of rock burst: a case study of Yima Yuejin coal mine, Henan, China. Chin J Geophys 57(8):2687–2700 (in Chinese)

Cai W, Dou LM, Gong SY, Li ZL, Yuan SS (2015) Quantitative analysis of seismic velocity tomography in rock burst hazard assessment. Nat Hazards 75(3):2453–2465

Chen XH, Li WQ, Yan XY (2012) Analysis on rock burst danger when fully mechanized caving coal face passed fault with deep mining. Saf Sci 50(4):645–648

Dou LM, He XQ (2007) Technique of classification forecasting rock burst in coal mines. J China Univ Min Technol 36(6):717–722 (in Chinese)

Dou LM, Zhao CG, Yang SG, Wu XR (2006) Prevention and control of rock burst in coal mine. China University of Mining and Technology Press, XuZhou (in Chinese)

Dou LM, Chen TJ, Gong SY, He H, Zhang SB (2012) Rockburst hazard determination by using computed tomography technology in deep workface. Saf Sci 50(4):736–740

Dou LM, Cai W, Gong SY, Han RJ, Liu J (2014) Dynamic risk assessment of rock burst based on the technology of seismic computed tomography detection. J China Coal Soc 39(2):238–244 (in Chinese)

Driad-Lebeau L, Lahaie F, Heib MA, Josien JP, Bigarré P, Noirel JF (2005) Seismic and geotechnical investigations following a rock burst in a complex French mining district. Int J Coal Geol 64(1):66–78

Eneva M, Mendecki AJ, Aswegen GV (1998) Seismic response of rock mass to blasting and rockburst potential. Int J Rock Mech Min Sci 35(4):390–391

Frankel (1995) Mapping seismic hazard in the central and eastern United States. Seismol Res Lett 66(4):8–21

Frankel AD, Mueller CS, Barnhard TP, Leyendecker EV, Wesson RL (2000) USGS national seismic hazard maps. Earthquake Spectra 16(1):1–19

Friedel MJ, Jackson MJ, Scott DF, Williams TJ, Olson MS (1995) 3-D tomographic imaging of anomalous conditions in a deep silver mine. J Appl Geophys 34(1):1–21

Friedel MJ, Scott DF, Williams TJ (1997) Temporal imaging of mine-induced stress change using seismic tomography. Eng Geol 46(2): 131–141

Gong SY, Dou LM, Cao AY, He H, Du TT, He J (2010) Study on optimal configuration of seismological observation network for coal mine. Chin J Geophys 53(2):457–465 (in Chinese)

Gong SY, Dou LM, He J, He H, Lu CP, Mu ZL (2012a) Study of correlation between stress and longitudinal wave velocity for deep burst tendency coal and rock samples in uniaxial cyclic loading and unloading experiment. Rock Soil Mech 33(1):41–47 (in Chinese)

Gong SY, Dou LM, Xu XJ, He J, Lu CP, He H (2012b) Experimental study on the correlation between stress and P-wave velocity for burst tendency coal-rock samples. J Min Saf Eng 29(1):67–71 (in Chinese)

Jiang YD, Pan YS, Jiang FX, Dou LM, Ju Y (2014) State of the art review on mechanism and prevention of coal bumps in China. J China Coal Soc 39(2):205–213 (in Chinese)

Kracke DW, Heinrich R (2004) Local seismic hazard assessment in areas of weak to moderate seismicity case study from Eastern Germany. Tectonophysics 390:45–55

Li ZL, Dou LM, Wang GF, Cai W, He J, Ding YL (2015) Risk evaluation of rock burst through theory of static and dynamic stresses superposition. J China Coal Soc 22(2):676–683 (in Chinese)

Lurka A (2005) Location of mining induced seismicity in zones of high P-wave velocity and in zones of high P-wave velocity gradient in Polish mines. Proceedings of the 6th international symposium on rock burst and seismicity in mines 3:479–483

PATYNSKA R (2013) The consequences of rock burst hazard for Silesian companies in Poland. Acta geodyn geometer 10(2):227–235

Peng SP, Ling BC, Liu SD (2002) Application of seismic tomography in longwall top-coal caving face. Chin J Rock Mech Eng 21(12):1786–1790 (in Chinese)

Senfaute G, Al-Heib M, Josien JP, Noirel JF (2014) Detection and monitoring of high stress concentration zones by numerical and micro-seismic methods. International Congress on Rock Mechanics 4(3): 1065–1070

Srinivasan C, Arora SK, Yaji RK (1997) Use of mining and seismological parameters as premonitors of rockbursts. Int J Rock Mech Min Sci 34(6):1001–1008

Wang Z, Bovik AC, Sheikh HR, Simoncelli EP (2004) Image quality assessment: from error visibility to structural similarity. IEEE Trans Image Process 13(4):600–612

Zhang MW, Shimada H, Sasaoka T, Matsui K, Dou LM (2013) Seismic energy distribution and hazard assessment in underground coal mines using statistical energy analysis. Int J Rock Mech Min Sci 64:192–200

Zhao YG, Li Q, Guo H, Jin HX, Wang CF (2000) Seismic attenuation tomography in frequency domain and its application to engineering. Sci China 43(4):431–438 (in Chinese)